

Then  $C_D$  is only 16 percent greater than the trailing-edge skin friction [compare with Eq. (7.27) for laminar flow].

The displacement thickness can be estimated from the one-seventh-power law and Eq. (7.12):

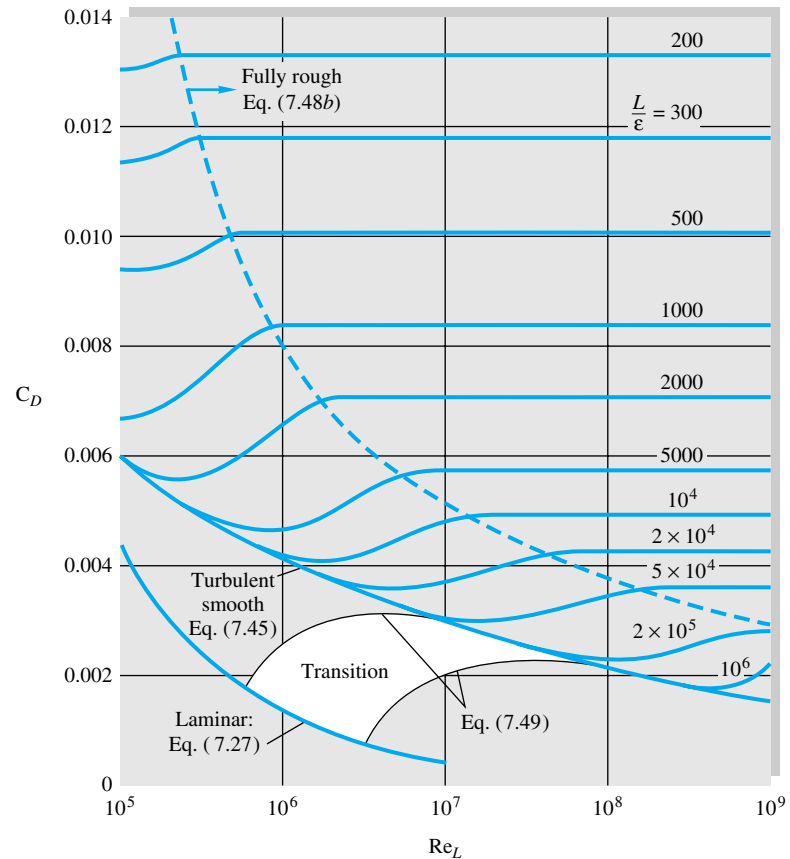
$$\delta^* \approx \int_0^\delta \left[ 1 - \left( \frac{y}{\delta} \right)^{1/7} \right] dy = \frac{1}{8} \delta \quad (7.46)$$

The turbulent flat-plate shape factor is approximately

$$H = \frac{\delta^*}{\theta} = \frac{\frac{1}{8}}{\frac{7}{72}} = 1.3 \quad (7.47)$$

These are the basic results of turbulent flat-plate theory.

Figure 7.6 shows flat-plate drag coefficients for both laminar- and turbulent-flow conditions. The smooth-wall relations (7.27) and (7.45) are shown, along with the effect of wall roughness, which is quite strong. The proper roughness parameter here is  $x/\epsilon$  or  $L/\epsilon$ , by analogy with the pipe parameter  $\epsilon/d$ . In the fully rough regime,  $C_D$  is independent of the Reynolds number, so that the drag varies exactly as  $U^2$  and is inde-



**Fig. 7.6** Drag coefficient of laminar and turbulent boundary layers on smooth and rough flat plates. This chart is the flat-plate analog of the Moody diagram of Fig. 6.13.

pendent of  $\mu$ . Reference 2 presents a theory of rough flat-plate flow, and Ref. 1 gives a curve fit for skin friction and drag in the fully rough regime:

$$c_f \approx \left( 2.87 + 1.58 \log \frac{x}{\epsilon} \right)^{-2.5} \quad (7.48a)$$

$$C_D \approx \left( 1.89 + 1.62 \log \frac{L}{\epsilon} \right)^{-2.5} \quad (7.48b)$$

Equation (7.48b) is plotted to the right of the dashed line in Fig. 7.6. The figure also shows the behavior of the drag coefficient in the transition region  $5 \times 10^5 < \text{Re}_L < 8 \times 10^7$ , where the laminar drag at the leading edge is an appreciable fraction of the total drag. Schlichting [1] suggests the following curve fits for these transition drag curves depending upon the Reynolds number  $\text{Re}_{\text{trans}}$  where transition begins:

$$C_D \approx \begin{cases} \frac{0.031}{\text{Re}_L^{1/7}} - \frac{1440}{\text{Re}_L} & \text{Re}_{\text{trans}} = 5 \times 10^5 \\ \frac{0.031}{\text{Re}_L^{1/7}} - \frac{8700}{\text{Re}_L} & \text{Re}_{\text{trans}} = 3 \times 10^6 \end{cases} \quad (7.49a)$$

$$(7.49b)$$

#### EXAMPLE 7.4

A hydrofoil 1.2 ft long and 6 ft wide is placed in a water flow of 40 ft/s, with  $\rho = 1.99$  slugs/ft<sup>3</sup> and  $\nu = 0.000011$  ft<sup>2</sup>/s. (a) Estimate the boundary-layer thickness at the end of the plate. Estimate the friction drag for (b) turbulent smooth-wall flow from the leading edge, (c) laminar turbulent flow with  $\text{Re}_{\text{trans}} = 5 \times 10^5$ , and (d) turbulent rough-wall flow with  $\epsilon = 0.0004$  ft.

#### Solution

**Part (a)** The Reynolds number is

$$\text{Re}_L = \frac{UL}{\nu} = \frac{(40 \text{ ft/s})(1.2 \text{ ft})}{0.000011 \text{ ft}^2/\text{s}} = 4.36 \times 10^6$$

Thus the trailing-edge flow is certainly turbulent. The maximum boundary-layer thickness would occur for turbulent flow starting at the leading edge. From Eq. (7.42),

$$\frac{\delta(L)}{L} = \frac{0.16}{(4.36 \times 10^6)^{1/7}} = 0.018$$

or

$$\delta = 0.018(1.2 \text{ ft}) = 0.0216 \text{ ft} \quad \text{Ans. (a)}$$

This is 7.5 times thicker than a fully laminar boundary layer at the same Reynolds number.

**Part (b)** For fully turbulent smooth-wall flow, the drag coefficient on one side of the plate is, from Eq. (7.45),

$$C_D = \frac{0.031}{(4.36 \times 10^6)^{1/7}} = 0.00349$$

Then the drag on both sides of the foil is approximately

$$D = 2C_D(\frac{1}{2}\rho U^2)bL = 2(0.00349)(\frac{1}{2})(1.99)(40)^2(6.0)(1.2) = 80 \text{ lb} \quad \text{Ans. (b)}$$

**Part (c)** With a laminar leading edge and  $\text{Re}_{\text{trans}} = 5 \times 10^5$ , Eq. (7.49a) applies:

$$C_D = 0.00349 - \frac{1440}{4.36 \times 10^6} = 0.00316$$

The drag can be recomputed for this lower drag coefficient:

$$D = 2C_D(\frac{1}{2}\rho U^2)bL = 72 \text{ lbf} \quad \text{Ans. (c)}$$

**Part (d)** Finally, for the rough wall, we calculate

$$\frac{L}{\epsilon} = \frac{1.2 \text{ ft}}{0.0004 \text{ ft}} = 3000$$

From Fig. 7.6 at  $\text{Re}_L = 4.36 \times 10^6$ , this condition is just inside the fully rough regime. Equation (7.48b) applies:

$$C_D = (1.89 + 1.62 \log 3000)^{-2.5} = 0.00644$$

and the drag estimate is

$$D = 2C_D(\frac{1}{2}\rho U^2)bL = 148 \text{ lbf} \quad \text{Ans. (d)}$$

This small roughness nearly doubles the drag. It is probable that the total hydrofoil drag is still another factor of 2 larger because of trailing-edge flow-separation effects.

## 7.5 Boundary Layers with Pressure Gradient<sup>3</sup>

The flat-plate analysis of the previous section should give us a good feeling for the behavior of both laminar and turbulent boundary layers, except for one important effect: flow separation. Prandtl showed that separation like that in Fig. 7.2b is caused by excessive momentum loss near the wall in a boundary layer trying to move downstream against increasing pressure,  $dp/dx > 0$ , which is called an *adverse pressure gradient*. The opposite case of decreasing pressure,  $dp/dx < 0$ , is called a *favorable gradient*, where flow separation can never occur. In a typical immersed-body flow, e.g., Fig. 7.2b, the favorable gradient is on the front of the body and the adverse gradient is in the rear, as discussed in detail in Chap. 8.

We can explain flow separation with a geometric argument about the second derivative of velocity  $u$  at the wall. From the momentum equation (7.19b) at the wall, where  $u = v = 0$ , we obtain

$$\left. \frac{\partial \tau}{\partial y} \right|_{\text{wall}} = \mu \left. \frac{\partial^2 u}{\partial y^2} \right|_{\text{wall}} = -\rho U \frac{dU}{dx} = \frac{dp}{dx}$$

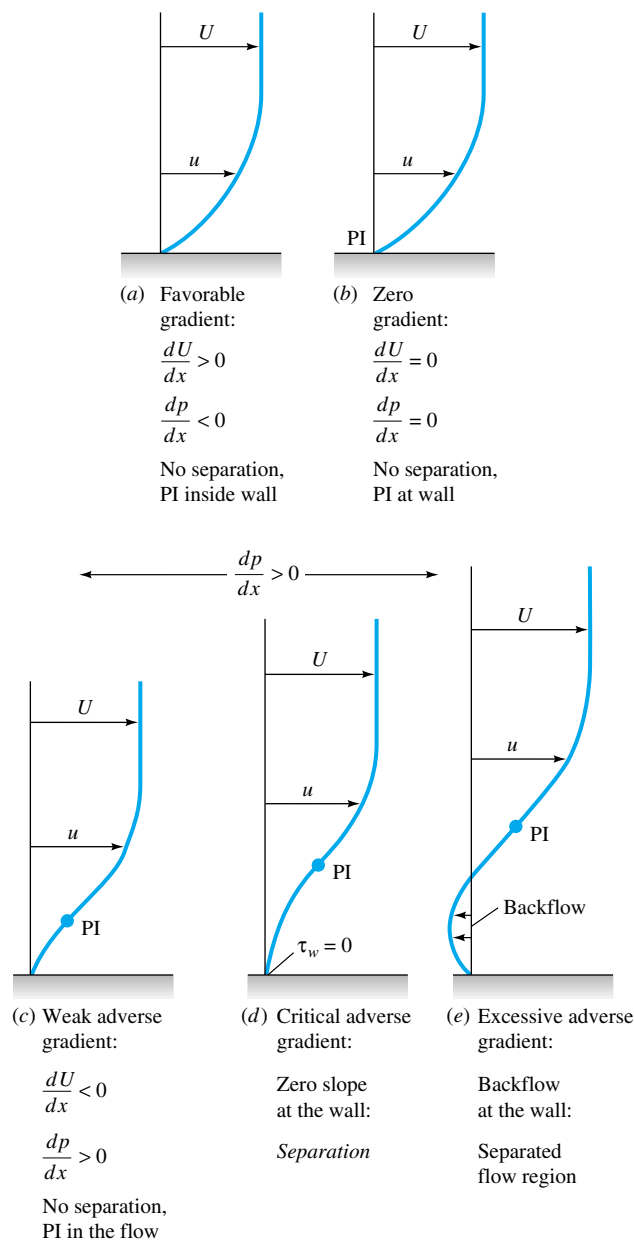
or

$$\left. \frac{\partial^2 u}{\partial y^2} \right|_{\text{wall}} = \frac{1}{\mu} \frac{dp}{dx} \quad (7.50)$$

<sup>3</sup>This section may be omitted without loss of continuity.

for either laminar or turbulent flow. Thus in an adverse gradient the second derivative of velocity is positive at the wall; yet it must be negative at the outer layer ( $y = \delta$ ) to merge smoothly with the mainstream flow  $U(x)$ . It follows that the second derivative must pass through zero somewhere in between, at a point of inflection, and any boundary-layer profile in an adverse gradient must exhibit a characteristic S shape.

Figure 7.7 illustrates the general case. In a favorable gradient (Fig. 7.7a) the profile



**Fig. 7.7** Effect of pressure gradient on boundary-layer profiles; PI = point of inflection.

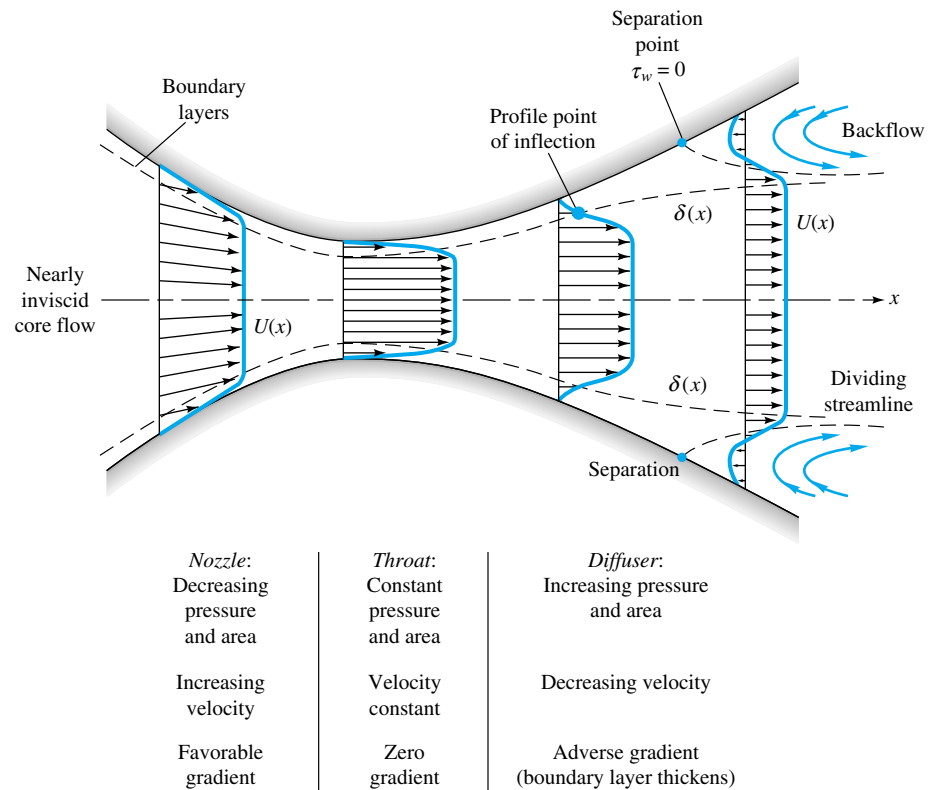
is very rounded, there is no point of inflection, there can be no separation, and laminar profiles of this type are very resistant to a transition to turbulence [1 to 3].

In a zero pressure gradient (Fig. 7.7*b*), e.g., flat-plate flow, the point of inflection is at the wall itself. There can be no separation, and the flow will undergo transition at  $Re_x$  no greater than about  $3 \times 10^6$ , as discussed earlier.

In an adverse gradient (Fig. 7.7*c* to *e*), a point of inflection (PI) occurs in the boundary layer, its distance from the wall increasing with the strength of the adverse gradient. For a weak gradient (Fig. 7.7*c*) the flow does not actually separate, but it is vulnerable to transition to turbulence at  $Re_x$  as low as  $10^5$  [1, 2]. At a moderate gradient, a critical condition (Fig. 7.7*d*) is reached where the wall shear is exactly zero ( $\partial u/\partial y = 0$ ). This is defined as the *separation point* ( $\tau_w = 0$ ), because any stronger gradient will actually cause backflow at the wall (Fig. 7.7*e*): the boundary layer thickens greatly, and the main flow breaks away, or separates, from the wall (Fig. 7.2*b*).

The flow profiles of Fig. 7.7 usually occur in sequence as the boundary layer progresses along the wall of a body. For example, in Fig. 7.2*a*, a favorable gradient occurs on the front of the body, zero pressure gradient occurs just upstream of the shoulder, and an adverse gradient occurs successively as we move around the rear of the body.

A second practical example is the flow in a duct consisting of a nozzle, throat, and diffuser, as in Fig. 7.8. The nozzle flow is a favorable gradient and never separates, nor



**Fig. 7.8** Boundary-layer growth and separation in a nozzle-diffuser configuration.

does the throat flow where the pressure gradient is approximately zero. But the expanding-area diffuser produces low velocity and increasing pressure, an adverse gradient. If the diffuser angle is too large, the adverse gradient is excessive, and the boundary layer will separate at one or both walls, with backflow, increased losses, and poor pressure recovery. In the diffuser literature [10] this condition is called *diffuser stall*, a term used also in airfoil aerodynamics (Sec. 7.6) to denote airfoil boundary-layer separation. Thus the boundary-layer behavior explains why a large-angle diffuser has heavy flow losses (Fig. 6.23) and poor performance (Fig. 6.28).

Presently boundary-layer theory can compute only up to the separation point, after which it is invalid. New techniques are now developed for analyzing the strong interaction effects caused by separated flows [5, 6].

## Laminar Integral Theory

Both laminar and turbulent theories can be developed from Kármán's general two-dimensional boundary-layer integral relation [7], which extends Eq. (7.33) to variable  $U(x)$

$$\frac{\tau_w}{\rho U^2} = \frac{1}{2} c_f = \frac{d\theta}{dx} + (2 + H) \frac{\theta}{U} \frac{dU}{dx} \quad (7.51)$$

where  $\theta(x)$  is the momentum thickness and  $H(x) = \delta^*(x)/\theta(x)$  is the shape factor. From Eq. (7.17) negative  $dU/dx$  is equivalent to positive  $dp/dx$ , that is, an adverse gradient.

We can integrate Eq. (7.51) to determine  $\theta(x)$  for a given  $U(x)$  if we correlate  $c_f$  and  $H$  with the momentum thickness. This has been done by examining typical velocity profiles of laminar and turbulent boundary-layer flows for various pressure gradients. Some examples are given in Fig. 7.9, showing that the shape factor  $H$  is a good indicator of the pressure gradient. The higher the  $H$ , the stronger the adverse gradient, and separation occurs approximately at

$$H \approx \begin{cases} 3.5 & \text{laminar flow} \\ 2.4 & \text{turbulent flow} \end{cases} \quad (7.52)$$

The laminar profiles (Fig. 7.9a) clearly exhibit the S shape and a point of inflection with an adverse gradient. But in the turbulent profiles (Fig. 7.9b) the points of inflection are typically buried deep within the thin viscous sublayer, which can hardly be seen on the scale of the figure.

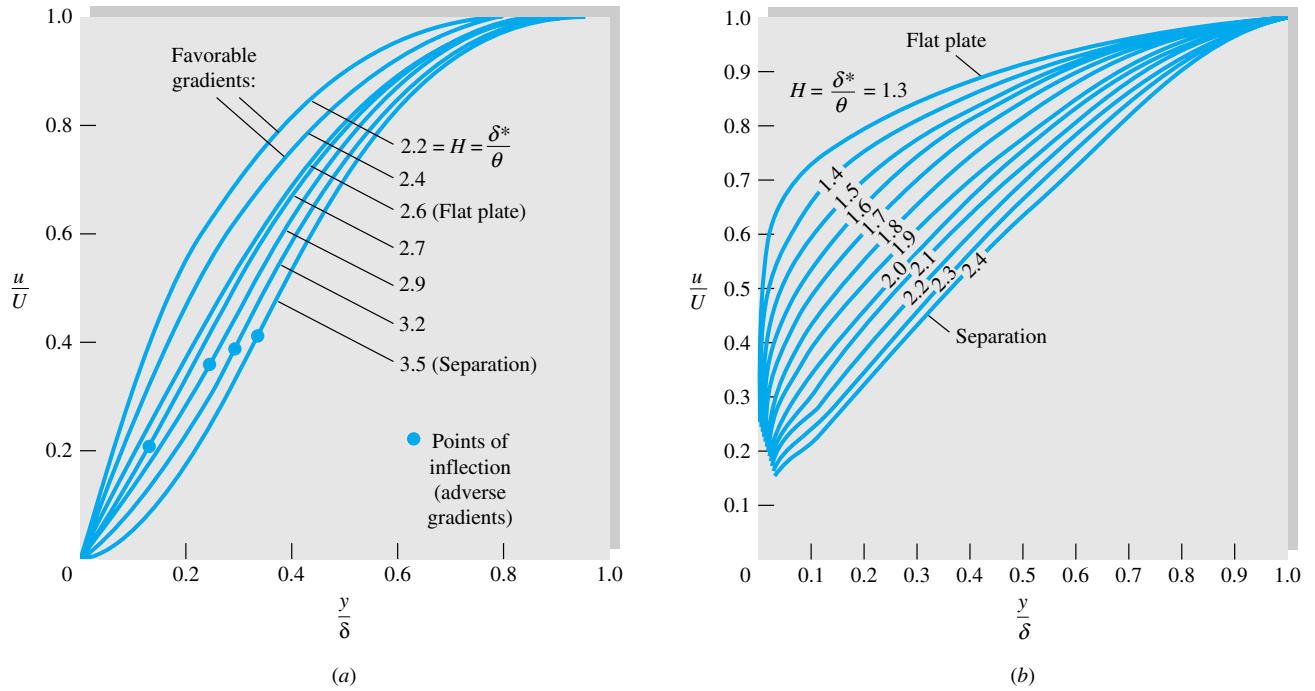
There are scores of turbulent theories in the literature, but they are all complicated algebraically and will be omitted here. The reader is referred to advanced texts [1, 2, 9].

For laminar flow, a simple and effective method was developed by Thwaites [11], who found that Eq. (7.51) can be correlated by a single dimensionless momentum-thickness variable  $\lambda$ , defined as

$$\lambda = \frac{\theta^2}{\nu} \frac{dU}{dx} \quad (7.53)$$

Using a straight-line fit to his correlation, Thwaites was able to integrate Eq. (7.51) in closed form, with the result

$$\theta^2 = \theta_0^2 \left( \frac{U_0}{U} \right)^6 + \frac{0.45\nu}{U^6} \int_0^x U^5 dx \quad (7.54)$$



**Fig. 7.9** Velocity profiles with pressure gradient: (a) laminar flow; (b) turbulent flow with adverse gradients.

where  $\theta_0$  is the momentum thickness at  $x = 0$  (usually taken to be zero). Separation ( $c_f = 0$ ) was found to occur at a particular value of  $\lambda$

$$\text{Separation:} \quad \lambda = -0.09 \quad (7.55)$$

Finally, Thwaites correlated values of the dimensionless shear stress  $S = \tau_w \theta / (\mu U)$  with  $\lambda$ , and his graphed result can be curve-fitted as follows:

$$S(\lambda) = \frac{\tau_w \theta}{\mu U} \approx (\lambda + 0.09)^{0.62} \quad (7.56)$$

This parameter is related to the skin friction by the identity

$$S \equiv \frac{1}{2} c_f \text{Re}_\theta \quad (7.57)$$

Equations (7.54) to (7.56) constitute a complete theory for the laminar boundary layer with variable  $U(x)$ , with an accuracy of  $\pm 10$  percent compared with exact digital-computer solutions of the laminar-boundary-layer equations (7.19). Complete details of Thwaites' and other laminar theories are given in Refs. 2 and 3.

As a demonstration of Thwaites' method, take a flat plate, where  $U = \text{constant}$ ,  $\lambda = 0$ , and  $\theta_0 = 0$ . Equation (7.54) integrates to

$$\theta^2 = \frac{0.45 \nu x}{U}$$

$$\text{or} \quad \frac{\theta}{x} = \frac{0.671}{\text{Re}_x^{1/2}} \quad (7.58)$$

This is within 1 percent of Blasius' exact solution, Eq. (7.30).

With  $\lambda = 0$ , Eq. (7.56) predicts the flat-plate shear to be

$$\frac{\tau_w \theta}{\mu U} = (0.09)^{0.62} = 0.225$$

$$\text{or} \quad c_f = \frac{2\tau_w}{\rho U^2} = \frac{0.671}{\text{Re}_x^{1/2}} \quad (7.59)$$

This is also within 1 percent of the Blasius result, Eq. (7.25). However, the general accuracy of this method is poorer than 1 percent because Thwaites actually "tuned" his correlation constants to make them agree with exact flat-plate theory.

We shall not compute any more boundary-layer details here, but as we go along, investigating various immersed-body flows, especially in Chap. 8, we shall use Thwaites' method to make qualitative assessments of the boundary-layer behavior.

---

### EXAMPLE 7.5

---

In 1938 Howarth proposed a linearly decelerating external-velocity distribution

$$U(x) = U_0 \left(1 - \frac{x}{L}\right) \quad (1)$$

as a theoretical model for laminar-boundary-layer study. (a) Use Thwaites' method to compute the separation point  $x_{\text{sep}}$  for  $\theta_0 = 0$ , and compare with the exact digital-computer solution  $x_{\text{sep}}/L = 0.119863$  given by H. Wipperman in 1966. (b) Also compute the value of  $c_f = 2\tau_w/(\rho U^2)$  at  $x/L = 0.1$ .

---

### Solution

---

**Part (a)** First note that  $dU/dx = -U_0/L = \text{constant}$ : Velocity decreases, pressure increases, and the pressure gradient is adverse throughout. Now integrate Eq. (7.54)

$$\theta^2 = \frac{0.45\nu}{U_0^6(1-x/L)^6} \int_0^x U_0^5 \left(1 - \frac{x}{L}\right)^5 dx = 0.075 \frac{\nu L}{U_0} \left[ \left(1 - \frac{x}{L}\right)^{-6} - 1 \right] \quad (2)$$

Then the dimensionless factor  $\lambda$  is given by

$$\lambda = \frac{\theta^2}{\nu} \frac{dU}{dx} = -\frac{\theta^2 U_0}{\nu L} = -0.075 \left[ \left(1 - \frac{x}{L}\right)^{-6} - 1 \right] \quad (3)$$

From Eq. (7.55) we set this equal to  $-0.09$  for separation

$$\lambda_{\text{sep}} = -0.09 = -0.075 \left[ \left(1 - \frac{x_{\text{sep}}}{L}\right)^{-6} - 1 \right]$$

$$\text{or} \quad \frac{x_{\text{sep}}}{L} = 1 - (2.2)^{-1/6} = 0.123 \quad \text{Ans. (a)}$$



This is less than 3 percent higher than Wipperman's exact solution, and the computational effort is very modest.

**Part (b)** To compute  $c_f$  at  $x/L = 0.1$  (just before separation), we first compute  $\lambda$  at this point, using Eq. (3)

$$\lambda(x = 0.1L) = -0.075[(1 - 0.1)^{-6} - 1] = -0.0661$$

Then from Eq. (7.56) the shear parameter is

$$S(x = 0.1L) = (-0.0661 + 0.09)^{0.62} = 0.099 = \frac{1}{2}c_f \text{Re}_\theta \quad (4)$$

We can compute  $\text{Re}_\theta$  in terms of  $\text{Re}_L$  from Eq. (2) or (3)

$$\frac{\theta^2}{L^2} = \frac{0.0661}{UL/\nu} = \frac{0.0661}{\text{Re}_L}$$

$$\text{or} \quad \text{Re}_\theta = 0.257 \text{Re}_L^{1/2} \quad \text{at} \quad \frac{x}{L} = 0.1$$

Substitute into Eq. (4):

$$0.099 = \frac{1}{2}c_f(0.257 \text{Re}_L^{1/2})$$

$$\text{or} \quad c_f = \frac{0.77}{\text{Re}_L^{1/2}} \quad \text{Re}_L = \frac{UL}{\nu} \quad \text{Ans. (b)}$$

We cannot actually compute  $c_f$  without the value of, say,  $U_0L/\nu$ .

## 7.6 Experimental External Flows

Boundary-layer theory is very interesting and illuminating and gives us a great qualitative grasp of viscous-flow behavior, but, because of flow separation, the theory does not generally allow a quantitative computation of the complete flow field. In particular, there is at present no satisfactory theory for the forces on an arbitrary body immersed in a stream flowing at an arbitrary Reynolds number. Therefore experimentation is the key to treating external flows.

Literally thousands of papers in the literature report experimental data on specific external viscous flows. This section gives a brief description of the following external-flow problems:

1. Drag of two-and three-dimensional bodies
  - a. Blunt bodies
  - b. Streamlined shapes
2. Performance of lifting bodies
  - a. Airfoils and aircraft
  - b. Projectiles and finned bodies
  - c. Birds and insects

For further reading see the goldmine of data compiled in Hoerner [12]. In later chapters we shall study data on supersonic airfoils (Chap. 9), open-channel friction (Chap. 10), and turbomachinery performance (Chap. 11).

## Drag of Immersed Bodies

Any body of any shape when immersed in a fluid stream will experience forces and moments from the flow. If the body has arbitrary shape and orientation, the flow will exert forces and moments about all three coordinate axes, as shown in Fig. 7.10. It is customary to choose one axis parallel to the free stream and positive downstream. The force on the body along this axis is called *drag*, and the moment about that axis the *rolling moment*. The drag is essentially a flow loss and must be overcome if the body is to move against the stream.

A second and very important force is perpendicular to the drag and usually performs a useful job, such as bearing the weight of the body. It is called the *lift*. The moment about the lift axis is called *yaw*.

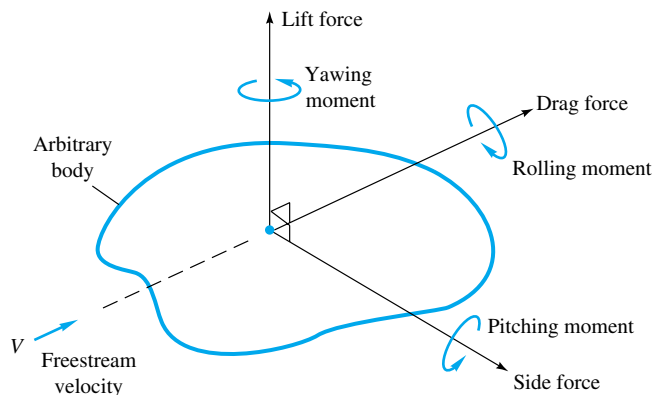
The third component, neither a loss nor a gain, is the *side force*, and about this axis is the *pitching moment*. To deal with this three-dimensional force-moment situation is more properly the role of a textbook on aerodynamics [for example, 13]. We shall limit the discussion here to lift and drag.

When the body has symmetry about the lift-drag axis, e.g., airplanes, ships, and cars moving directly into a stream, the side force, yaw, and roll vanish, and the problem reduces to a two-dimensional case: two forces, lift and drag, and one moment, pitch.

A final simplification often occurs when the body has two planes of symmetry, as in Fig. 7.11. A wide variety of shapes such as cylinders, wings, and all bodies of revolution satisfy this requirement. If the free stream is parallel to the intersection of these two planes, called the *principal chord line of the body*, the body experiences drag only, with no lift, side force, or moments.<sup>4</sup> This type of degenerate one-force drag data is what is most commonly reported in the literature, but if the free stream is not parallel to the chord line, the body will have an unsymmetric orientation and all three forces and three moments can arise in principle.

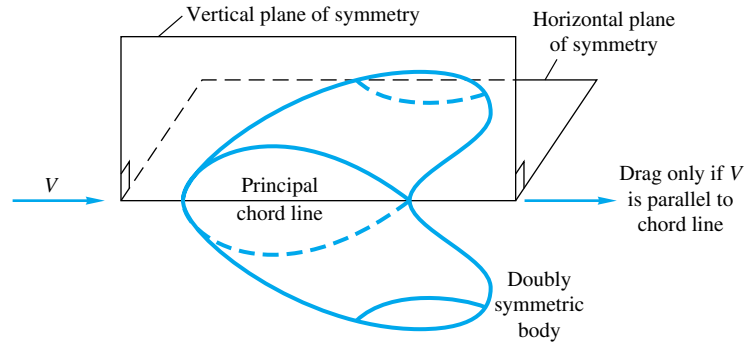
In low-speed flow past geometrically similar bodies with identical orientation and relative roughness, the drag coefficient should be a function of the body Reynolds number

$$C_D = f(\text{Re}) \quad (7.60)$$



**Fig. 7.10** Definition of forces and moments on a body immersed in a uniform flow.

<sup>4</sup>In bodies with shed vortices, such as the cylinder in Fig. 5.2, there may be *oscillating* lift, side force, and moments, but their mean value is zero.



**Fig. 7.11** Only the drag force occurs if the flow is parallel to both planes of symmetry.

The Reynolds number is based upon the free-stream velocity  $V$  and a characteristic length  $L$  of the body, usually the chord or body length parallel to the stream

$$\text{Re} = \frac{VL}{\nu} \quad (7.61)$$

For cylinders, spheres, and disks, the characteristic length is the diameter  $D$ .

### Characteristic Area

Drag coefficients are defined by using a characteristic area  $A$  which may differ depending upon the body shape:

$$C_D = \frac{\text{drag}}{\frac{1}{2}\rho V^2 A} \quad (7.62)$$

The factor  $\frac{1}{2}$  is our traditional tribute to Euler and Bernoulli. The area  $A$  is usually one of three types:

1. *Frontal area*, the body as seen from the stream; suitable for thick, stubby bodies, such as spheres, cylinders, cars, missiles, projectiles, and torpedoes.
2. *Planform area*, the body area as seen from above; suitable for wide, flat bodies such as wings and hydrofoils.
3. *Wetted area*, customary for surface ships and barges.

In using drag or other fluid-force data, it is important to note what length and area are being used to scale the measured coefficients.

### Friction Drag and Pressure Drag

As we have mentioned, the theory of drag is weak and inadequate, except for the flat plate. This is because of flow separation. Boundary-layer theory can predict the separation point but cannot accurately estimate the (usually low) pressure distribution in the separated region. The difference between the high pressure in the front stagnation region and the low pressure in the rear separated region causes a large drag contribution called *pressure drag*. This is added to the integrated shear stress or *friction drag* of the body, which it often exceeds:

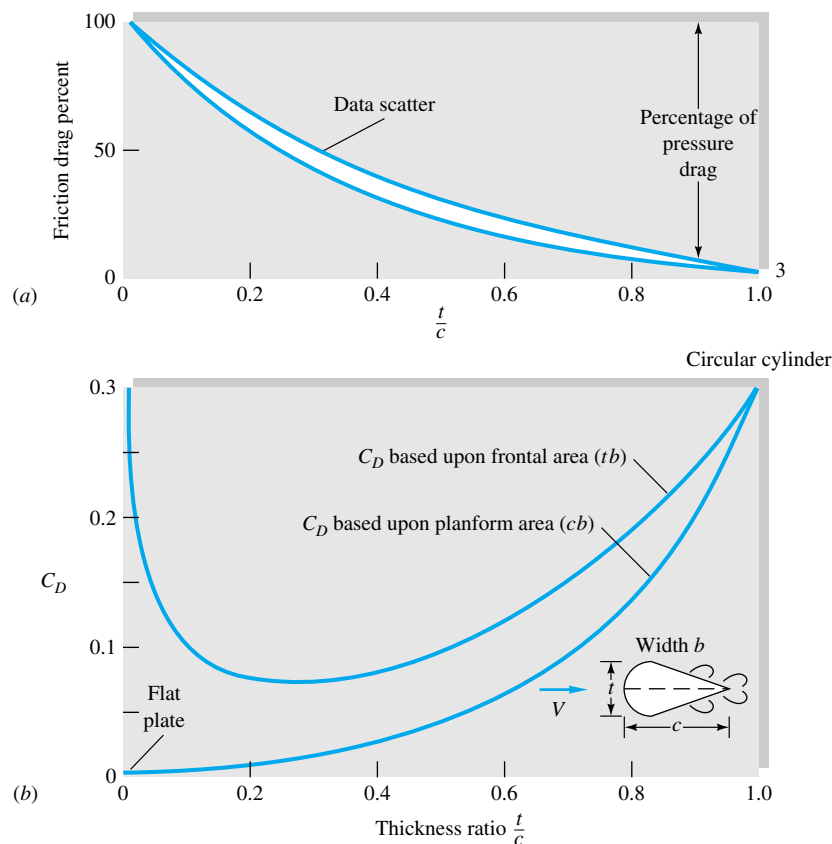
$$C_D = C_{D,\text{press}} + C_{D,\text{fric}} \quad (7.63)$$

The relative contribution of friction and pressure drag depends upon the body's shape, especially its thickness. Figure 7.12 shows drag data for a streamlined cylinder of very large depth into the paper. At zero thickness the body is a flat plate and exhibits 100 percent friction drag. At thickness equal to the chord length, simulating a circular cylinder, the friction drag is only about 3 percent. Friction and pressure drag are about equal at thickness  $t/c = 0.25$ . Note that  $C_D$  in Fig. 7.12b looks quite different when based upon frontal area instead of planform area, planform being the usual choice for this body shape. The two curves in Fig. 7.12b represent exactly the same drag data.

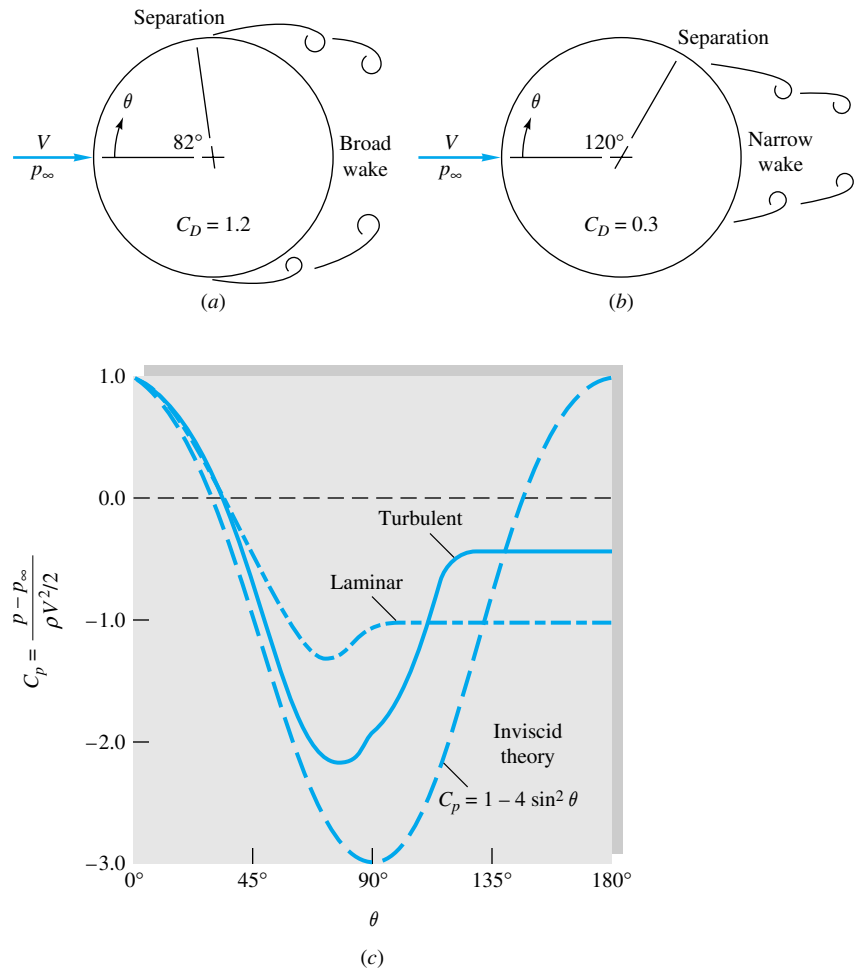
Figure 7.13 illustrates the dramatic effect of separated flow and the subsequent failure of boundary-layer theory. The theoretical inviscid pressure distribution on a circular cylinder (Chap. 8) is shown as the dashed line in Fig. 7.13c:

$$C_p = \frac{p - p_\infty}{\frac{1}{2}\rho V^2} = 1 - 4 \sin^2 \theta \quad (7.64)$$

where  $p_\infty$  and  $V$  are the pressure and velocity, respectively, in the free stream. The actual laminar and turbulent boundary-layer pressure distributions in Fig. 7.13c are startlingly different from those predicted by theory. Laminar flow is very vulnerable to the adverse gradient on the rear of the cylinder, and separation occurs at  $\theta = 82^\circ$ , which



**Fig. 7.12** Drag of a streamlined two-dimensional cylinder at  $Re_c = 10^6$ : (a) effect of thickness ratio on percentage of friction drag; (b) total drag versus thickness when based upon two different areas.



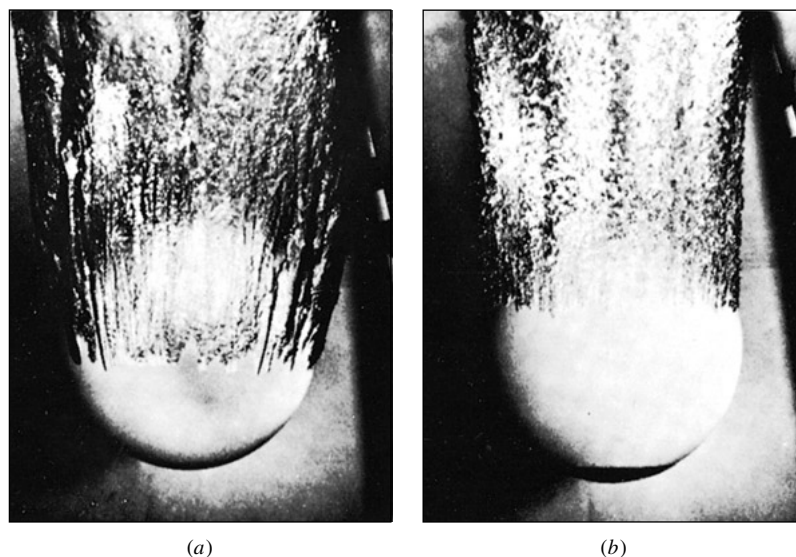
**Fig. 7.13** Flow past a circular cylinder: (a) laminar separation; (b) turbulent separation; (c) theoretical and actual surface-pressure distributions.

certainly could not have been predicted from inviscid theory. The broad wake and very low pressure in the separated laminar region cause the large drag  $C_D = 1.2$ .

The turbulent boundary layer in Fig. 7.13b is more resistant, and separation is delayed until  $\theta = 120^\circ$ , with a resulting smaller wake, higher pressure on the rear, and 75 percent less drag,  $C_D = 0.3$ . This explains the sharp drop in drag at transition in Fig. 5.3.

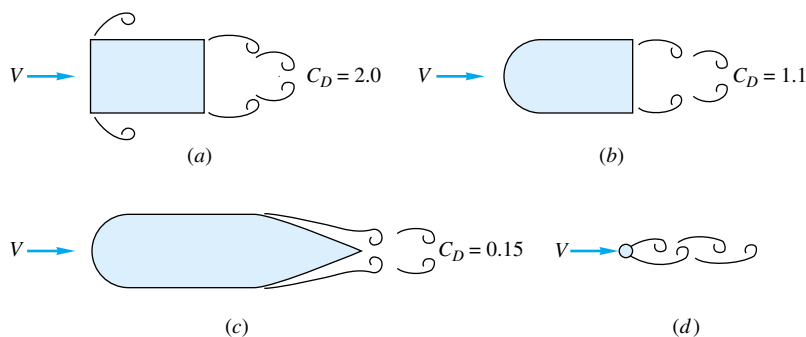
The same sharp difference between vulnerable laminar separation and resistant turbulent separation can be seen for a sphere in Fig. 7.14. The laminar flow (Fig. 7.14a) separates at about  $80^\circ$ ,  $C_D = 0.5$ , while the turbulent flow (Fig. 7.14b) separates at  $120^\circ$ ,  $C_D = 0.2$ . Here the Reynolds numbers are exactly the same, and the turbulent boundary layer is induced by a patch of sand roughness at the nose of the ball. Golf balls fly in this range of Reynolds numbers, which is why they are deliberately dimpled – to induce a turbulent boundary layer and lower drag. Again we would find the actual pressure distribution on the sphere to be quite different from that predicted by inviscid theory.

**Fig. 7.14** Strong differences in laminar and turbulent separation on an 8.5-in bowling ball entering water at 25 ft/s: (a) smooth ball, laminar boundary layer; (b) same entry, turbulent flow induced by patch of nose-sand roughness. (U.S. Navy photograph, Ordnance Test Station, Pasadena Annex.)



In general, we cannot overstate the importance of body streamlining to reduce drag at Reynolds numbers above about 100. This is illustrated in Fig. 7.15. The rectangular cylinder (Fig. 7.15a) has rampant separation at all sharp corners and very high drag. Rounding its nose (Fig. 7.15b) reduces drag by about 45 percent, but  $C_D$  is still high. Streamlining its rear to a sharp trailing edge (Fig. 7.15c) reduces its drag another 85 percent to a practical minimum for the given thickness. As a dramatic contrast, the circular cylinder (Fig. 7.15d) has one-eighth the thickness and one-three-hundredth the cross section (c) (Fig. 7.15c), yet it has the same drag. For high-performance vehicles and other moving bodies, the name of the game is drag reduction, for which intense research continues for both aerodynamic and hydrodynamic applications [20, 39].

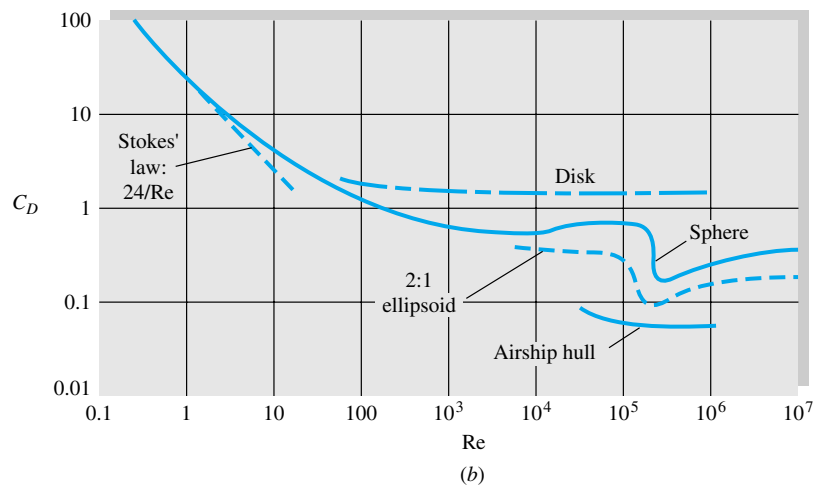
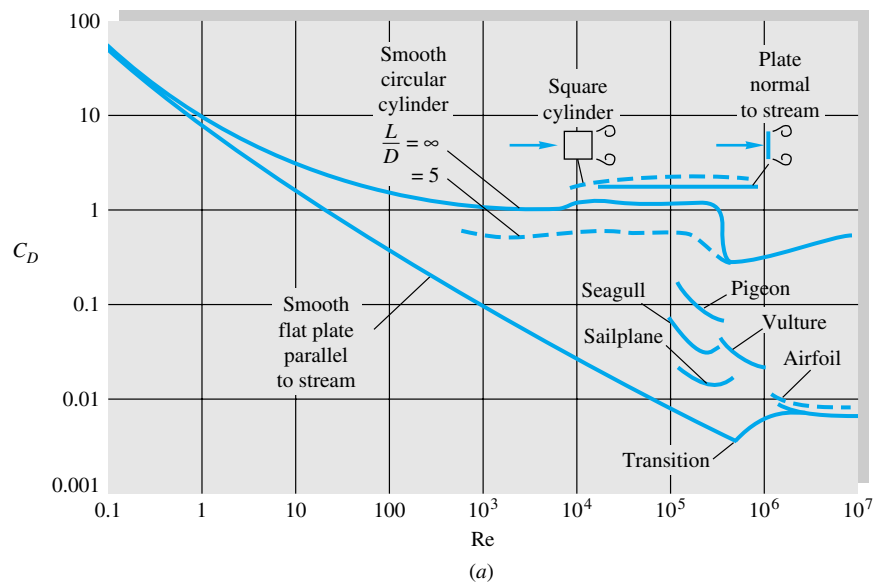
The drag of some representative wide-span (nearly two-dimensional) bodies is shown versus the Reynolds number in Fig. 7.16a. All bodies have high  $C_D$  at very low (*creeping flow*)  $Re \leq 1.0$ , while they spread apart at high Reynolds numbers according to



**Fig. 7.15** The importance of streamlining in reducing drag of a body ( $C_D$  based on frontal area): (a) rectangular cylinder; (b) rounded nose; (c) rounded nose and streamlined sharp trailing edge; (d) circular cylinder with the same drag as case (c).




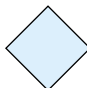

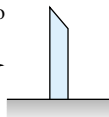

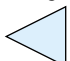
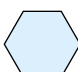

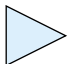
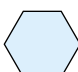
their degree of streamlining. All values of  $C_D$  are based on the planform area except the plate normal to the flow. The birds and the sailplane are, of course, not very two-dimensional, having only modest span length. Note that birds are not nearly as efficient as modern sailplanes or airfoils [14, 15].

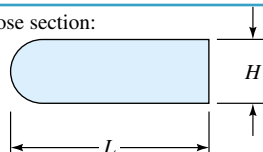
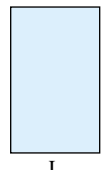
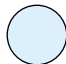



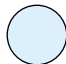



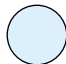



Table 7.2 gives a few data on drag, based on frontal area, of two-dimensional bodies of various cross section, at  $Re \geq 10^4$ . The sharp-edged bodies, which tend to cause flow separation regardless of the character of the boundary layer, are insensitive to the Reynolds number. The elliptic cylinders, being smoothly rounded, have the laminar-to-turbulent transition effect of Figs. 7.13 and 7.14 and are therefore quite sensitive to whether the boundary layer is laminar or turbulent.



**Fig. 7.16** Drag coefficients of smooth bodies at low Mach numbers: (a) two-dimensional bodies; (b) three-dimensional bodies. Note the Reynolds-number independence of blunt bodies at high  $Re$ .

**Table 7.2** Drag of Two-Dimensional Bodies at  $Re \geq 10^4$

Shape	$C_D$ based on frontal area	Shape	$C_D$ based on frontal area	Shape	$C_D$ based on frontal area
Square cylinder: 	2.1	Half-cylinder: 	1.2	Plate: 	2.0
	1.6		1.7	Thin plate normal to a wall: 	1.4
Half tube: 	1.2	Equilateral triangle: 	1.6	Hexagon: 	1.0
	2.3		2.0		0.7

Shape	$C_D$ based on frontal area																		
Rounded nose section: 	<table><tr><td><math>L/H:</math></td><td>0.5</td><td>1.0</td><td>2.0</td><td>4.0</td><td>6.0</td></tr><tr><td><math>C_D:</math></td><td>1.16</td><td>0.90</td><td>0.70</td><td>0.68</td><td>0.64</td></tr></table>	$L/H:$	0.5	1.0	2.0	4.0	6.0	$C_D:$	1.16	0.90	0.70	0.68	0.64						
$L/H:$	0.5	1.0	2.0	4.0	6.0														
$C_D:$	1.16	0.90	0.70	0.68	0.64														
Flat nose section 	<table><tr><td><math>L/H:</math></td><td>0.1</td><td>0.4</td><td>0.7</td><td>1.2</td><td>2.0</td><td>2.5</td><td>3.0</td><td>6.0</td></tr><tr><td><math>C_D:</math></td><td>1.9</td><td>2.3</td><td>2.7</td><td>2.1</td><td>1.8</td><td>1.4</td><td>1.3</td><td>0.9</td></tr></table>	$L/H:$	0.1	0.4	0.7	1.2	2.0	2.5	3.0	6.0	$C_D:$	1.9	2.3	2.7	2.1	1.8	1.4	1.3	0.9
$L/H:$	0.1	0.4	0.7	1.2	2.0	2.5	3.0	6.0											
$C_D:$	1.9	2.3	2.7	2.1	1.8	1.4	1.3	0.9											
Elliptical cylinder:	<table><tr><th></th><th>Laminar</th><th>Turbulent</th></tr><tr><td>1:1 </td><td>1.2</td><td>0.3</td></tr><tr><td>2:1 </td><td>0.6</td><td>0.2</td></tr><tr><td>4:1 </td><td>0.35</td><td>0.15</td></tr><tr><td>8:1 </td><td>0.25</td><td>0.1</td></tr></table>		Laminar	Turbulent	1:1 	1.2	0.3	2:1 	0.6	0.2	4:1 	0.35	0.15	8:1 	0.25	0.1			
	Laminar	Turbulent																	
1:1 	1.2	0.3																	
2:1 	0.6	0.2																	
4:1 	0.35	0.15																	
8:1 	0.25	0.1																	